# From Individual to Swarm Dynamics of Motile Photokinetic Organisms

J. Morales
*Departamento de Matemática, Universidad Tecnológica Metropolitana, Santiago, Chile*

P. Muñoz
*Departamento de Matemática, Universidad Técnica Federico Santa María, Santiago, Chile*

D. Noto
*Faculty of Engineering, Hokkaido University, Sapporo 060-8628, Japan*
*and Department of Earth and Environmental Science, University of Pennsylvania, Philadelphia, Pennsylvania 19104, USA*

H. N. Ulloa*
*Department of Earth and Environmental Science, University of Pennsylvania, Philadelphia, Pennsylvania 19104, USA*

F. Guzmán-Lastra†
*Departamento de Física, Facultad de Ciencias, Universidad de Chile, Santiago, Chile*

(Received 23 June 2025; accepted 6 April 2026; published 30 April 2026)

The day–night cycle drives the largest biomass migration on Earth: the diel vertical migration (DVM) of aquatic organisms. Here, we present a three-dimensional agent-based model that incorporates photokinesis, gyrotaxis, and stochastic reorientation to explore how individual-level swimming behaviors give rise to population-scale DVM patterns. By solving Langevin equations for swarms of swimmers, we identify four distinct regimes—*surface accumulation*, *shallow DVM*, *deep DVM*, and *sinking*—governed by two key dimensionless parameters: the Péclet number (Pe), representing motility persistence, and the vertical swimming asymmetry ratio ($W = w_{\text{down}}/w_{\text{up}}$), encoding photokinetic bias. These regimes emerge from nonlinear interactions between light-driven navigation and active noise, diagnosed through topological and statistical features of vertical distributions. A critical feedback is uncovered: upward-biased swimming ($W < 1$) promotes surface aggregation, while excessive downward bias ($W > 1$) leads to irreversible sinking. Analytical estimates link regime boundaries to gyrotactic alignment and velocity reversals. Together, our results provide a mechanistic framework to interpret DVM diversity and emphasize the central role of light gradients—beyond absolute intensity—in shaping ecological self-organization.

DOI: 10.1103/b3m3-2ffz

## I. INTRODUCTION

The diurnal cycle of sunlight drives the largest coordinated swimming of organisms in Earth's aquatic ecosystems [1,2]. Each day, swarms of motile plankton ascend at dusk and descend at dawn, forming a global-scale biological wave that shapes biogeochemical cycles, trophic dynamics and climate [2–4]. This phenomenon—known as diel vertical migration (DVM) [5,6]—is primarily governed by light cues and reflects an evolutionary trade-off between predator avoidance, nutrient acquisition, and photosynthetic efficiency [7–12]. At the organismal level, DVM arises from the power of plankton to swim guided by light, gravity, and buoyancy [13–20]. These microscale behaviors self-organize into large-scale patterns, further modulated by stratification, shear, and convection [21–30]. Despite over two centuries of research, the mechanisms driving the diversity of collective DVM behaviors—ranging shallow to deep excursions and tightly clustered to dispersed distributions—remain difficult to measure and to integrate into models, hindering our ability to predict how organisms respond to rapidly changing environmental conditions [6].

To capture the multiscale dynamics of collective swimming, two principal modeling frameworks have been developed: continuum models [2,31–33] and agent-based models (ABM) [34–37]. Continuum models treat organisms concentration as a continuous field governed by advection–diffusion transport equations [31,38–40], where phototactic behavior is represented by drift terms and dispersion by turbulence-dependent diffusivity [41–46]. While these models offer analytical tractability and capture large-scale DVM patterns, they often neglect key organism-scale mechanisms such as adaptive motility and light signal integration—limiting

*Contact author: ulloa@sas.upenn.edu
†Contact author: fguzman@uchile.cl

*Published by the American Physical Society under the terms of the Creative Commons Attribution 4.0 International license. Further distribution of this work must maintain attribution to the author(s) and the published article's title, journal citation, and DOI.*

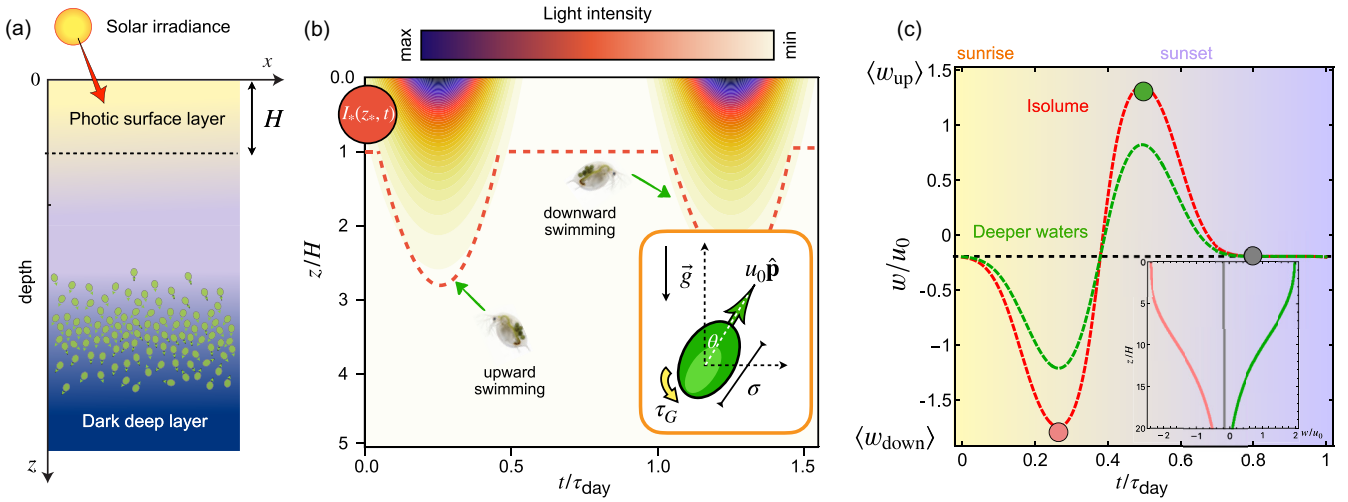



FIG. 1. Diel vertical migration of motile photokinetic organisms. (a) Schematic of a plankton colony initially distributed uniformly over the water column $L_z$. The depth $H$ denotes the nocturnal niche where organisms preferentially cluster. (b) Prescribed spatiotemporal light field $I(z,t)$: intensity is maximal at the surface $I_0$ and decreases exponentially with depth $z$, while its surface value varies over daytime, reaching a minimum at night. Motile plankton communities (e.g., *Daphnia magna*) follows a preferred light intensity niche $I_*$; the corresponding target depth $z_*(t)$ (red dashed line) varies over daytime. Inset: swimmers are modeled as spheres of diameter $\sigma$ moving with characteristic speed $u_0$ and orientation $\hat{\mathbf{p}}(t)$, subjected to gyrotactic reorientation with timescale $\tau_G$ and rotational Brownian motion $D_R$. We define the individual Péclet number as $\mathrm{Pe} = u_0/(D_R\,\sigma)$, with $D_R \propto \tau_G^{-1}$. (c) Light-controlled vertical swimming strategy defined in Eq. (7). The red dashed line shows an example of the rate of change of the target nondimensional velocity $\dot{z}_*/u_0$. The green dashed line shows the nondimensional vertical nondimensional velocity $w/u_0$ for a swimmer located deeper than $z_*$. Inset: depth profile of the vertical velocity distribution at three representative times, midday (pink), sunset (green), and night (gray). The swimming strategy is parameterized by the vertical velocity ratio, $W = w_{\mathrm{down}}/w_{\mathrm{up}}$.

their capacity to link mechanical behaviors from the organism to the swarm. Agent-based models take a "bottom-up" approach [34], explicitly framing the Lagrangian trajectories of self-propelled agents that respond to local light cues via phototaxis, photokinesis (modulation of swimming speed by light intensity), stochastic fluctuations, and circadian switching [2,23,26,47–50]. These models reveal how sensory-motor coupling and environmental feedback drive complex, emergent dynamics. Yet, despite their mechanistic richness, existing agent-based models have not quantitatively bridged organism-scale behavior with population-scale migration patterns [34,35,51]. Key questions remain: To what extent bottom-up ABM approach can reproduce large-scale collective dynamics of light-driven motile organisms observed in nature? How do swimming organisms—whose physiology is encoded with vertical-velocity modulation, gyrotaxis, and Brownian diffusion—respond to circadian light signals?

Here, we introduce an ABM framework and present numerical simulations of motile organisms encoded with photokinesis, gyrotaxis, and Brownian motion. These organism-scale behaviors give rise to a constellation of self-organized, population-level patterns. These patterns are regulated by spatiotemporal variations in light and captured through two key dimensionless parameters: the Péclet number (Pe), quantifying the balance between directed motion and rotational diffusion, and the vertical swimming asymmetry ratio ($W$), which measures vertical motility bias [52]. We report a previously unrecognized role for the interplay between photokinetic speed modulation and gyrotactic alignment in shaping both organisms trajectory and DVM structures. Our findings provides a mechanistic model for understanding individual and collective behaviors of light-sensitive swimmers such as zooplankton, and a framework for designing and controlling photosensitive active matter.

## II. ABM FRAMEWORK

Light is widely recognized as the primary environmental cue regulating DVM in both marine and lacustrine systems [5]. During daylight hours, many species position themselves at depths corresponding to a "dusky-light niche," defined by a critical isolume intensity $I_*$ located at a time-dependent depth $z_*(t)$ [19,31]. At night, swimming organisms ascend toward the upper water column or aggregate near the thermocline, where zooplankton typically graze on phytoplankton. Vertical migration is thus tightly coupled to light availability, as demonstrated by their rapid responses to changes in sunlight and moonlight intensity [53,54]. In our model, a swarm of $N$ motile organisms follows a swimming strategy modulated by a circadian spatiotemporal light field in a three-dimensional water column, in which intensity decreases with depth, and varies through daytime (Fig. 1). Each organism is treated as an active photokinetic agent of spherical shape and size $\sigma$ that self-propels at a characteristic speed $u_0$ and adjusts its vertical velocity to maintain alignment with the isolume $I_*(t,z)$ [31,49,55]. For simplicity, organisms do not growth nor die. Moreover, the effect of turbulence—inherent of natural environments—is not explicitly accounted by the model. Instead, organisms are built in with a Brownian behavior, whose intensity is described in terms of a rotational diffusion. Such a stochastic dynamic is boosted when organisms experience shear. Thus, the motion of the $i$th swimmer with

position vector $\mathbf{r}_i(t)$ and orientation $\hat{\mathbf{p}}_i(t)$, is described by the Langevine equations of motion,

$$\dot{\mathbf{r}}_i = u_0\hat{\mathbf{p}}_i - \frac{\nabla_{\mathbf{r}_i}U_i}{\gamma_T} + w(I(t,z))\hat{\mathbf{k}}, \tag{1}$$

$$\dot{\hat{\mathbf{p}}}_i = \frac{1}{\gamma_R}\boldsymbol{\xi}_{i,R}\times\hat{\mathbf{p}}_i + \frac{\hat{\mathbf{k}} - (\hat{\mathbf{k}}\cdot\hat{\mathbf{p}}_i)\hat{\mathbf{p}}_i}{\tau_G}. \tag{2}$$

The term "$u_0\hat{\mathbf{p}}_i$" in Eq. (1) characterizes the organims's self-propulsion, whereas $U_i$ denotes the excluded volume pair interactions,

$$U_i = \sum_{i\neq j} U^{ij}_{\mathrm{WCA}}(\mathbf{r}_i(t), \mathbf{r}_j(t)), \tag{3}$$

where $\mathbf{r}_j(t)$ denotes the position of the $j$th particle at time $t$, and $U^{ij}_{\mathrm{WCA}}$ is the Weeks-Chandler-Andersen (WCA) pair potential, given by

$$U^{ij}_{\mathrm{WCA}} = \begin{cases} 4\varepsilon\left[\left(\frac{\sigma}{r_{ij}}\right)^{12} - \left(\frac{\sigma}{r_{ij}}\right)^{6}\right] & r_{ij}\leqslant\sigma_r, \\ 0 & \text{otherwise.}\end{cases} \tag{4}$$

Here, $\gamma_T$ is the translational Stokes friction coefficient, $\sigma_r = 2^{1/6}\sigma$ is the contact radius, $r_{ij} = |\mathbf{r}_i - \mathbf{r}_j|$ corresponds to the distance between the agent $i$ and $j$, and $\varepsilon$ is an energy interaction strength.

The third term in Eq. (1), $w(I(t,z))\hat{\mathbf{k}}$, encodes the photokinetic response of the agent in the vertical direction. This term does not set the orientation toward or away from the light source (phototaxis [45,50]); rather, it modulates the vertical swimming speed (i.e., the bias in vertical motion) as a function of the local light intensity $I(t,z)$. This represents a biologically plausible control through which microswimmers adjust vertical positioning via stroke modulation, changes in helical pitch, or buoyancy-like adjustments [24,56–58]. Accordingly, agents adjust their vertical velocity depending on whether their local light exposure is above or below a threshold value $I_*(t,z)$. The latter is implemented by establishing a functional relationship between $w$ and the local light intensity, such that motion is controlled by intensity thresholds rather than by resolving the vector direction of incoming light.

Following the photokinetic model proposed by Richards *et al.* [31], we first define the light intensity field as follows:

$$I(t,z) = I_0\,\tau(t)\,\zeta(z), \tag{5}$$

where $I_0$ denotes the maximum light intensity achieved at the surface ($z=0$). The function $\zeta(z) = \exp(-k_d z)$ describes the vertical light distribution following the Beer–Lambert law, where $k_d$ is the bulk light attenuation coefficient that controls how deeply light penetrates into the water column and thus the depth of the threshold isolume $I_*$ [5,31]. The temporal variation of the light intensity is modeled by a smooth positive-defined function representing a canonical day-night cycle of period $\tau_{\mathrm{day}}$, e.g., Ref. [31]: $\tau(t) = a[1-\sin(2\pi t/\tau_{\mathrm{day}} - \phi)]^b$, and dimensionless model parameters $a = 1/16$, $b = 4$, and $\phi = \pi$.

To stay within a preferred, light-modulated depth niche, organisms continuously sense local light conditions, and adjust their vertical swimming direction to approach a target depth $z_*(t)$ (e.g., a preferred isolume) [5,31]. During daytime, the target depth is defined implicitly by the preferred light level $I_*$ via $I(t,z) = I_*$, so that organisms swim upward or downward depending on whether the local light intensity exceeds or falls below $I_*$. At night, by contrast, organisms migrate toward a preferred shallow depth $H$ near the surface, representing a typical nocturnal feeding niche [5]:

$$z_*(t) = \begin{cases} \frac{1}{k_d}\log\left[\frac{I_0}{I_*}\tau(t)\right] + H, & \text{daytime,} \\ H, & \text{nighttime,}\end{cases} \tag{6}$$

where daytime and nighttime correspond to the periodic intervals $t\in[k\,\tau_{\mathrm{day}}, (k+1/2)\,\tau_{\mathrm{day}}]$ and $t\in[(k+1/2)\,\tau_{\mathrm{day}}, (k+1)\,\tau_{\mathrm{day}}]$, respectively, with $k\in\mathbb{N}_0 = \{0,1,2,\dots\}$.

Therefore, if an organism is above $z_*$, then they are expected to swim downward or perform positive sinking, which here is represented as diving at a rate $w_{\mathrm{down}}$ until it reaches or falls below the isolume $I_*$. Then, a preferred light intensity mechanism response follows. From sunrise to midday—when the depth $z_*(t)$ of the isolume $I_*$ deepens—organisms are expected to swim downward at a dimensionless speed $w_{\mathrm{down}}/u_0$. After midday, as the depth of the isolume $I_*$ ascends, swimmers are expected to reverse direction and start ascending at a dimensionless speed $w_{\mathrm{up}}/u_0$ until sunset. During nighttime, light-guided vertical migration ceases $w/u_0\approx 0$, and organisms remain statistically at the fixed depth $H$ until the next dawn begins. As an example, Fig. 1(c) shows the swimming strategy of organisms that swim faster downward than upward [59]. Green trajectories represent motion when an organism depth $z_{\mathrm{org}}$ is deeper than the target depth $z_*$, whereas red trajectories correspond to the case $z_{\mathrm{org}} = z_*$, i.e., organisms that follow the depth of the niche isolume. The inset in Fig. 1(c) highlights depth-dependent velocity changes with pink, green, and gray curves, corresponding to specific times marked by colored circles in the main panel. These trajectories illustrate the ability of organisms to track their preferred isolume $I_*$ depending on both their propulsion speed and position $z_{\mathrm{org}}$ relative to $z_*(t)$.

Mathematically, the photokinetic swimming strategy is formulated as follows:

$$w(z,t) = \begin{cases} -w_{\mathrm{down}} & \text{if } I\geqslant I_* \\ \frac{1}{2}w_{\mathrm{up}}[1+\tanh(A_1)]+ & \\ \frac{1}{2}w_{\mathrm{down}}[2\tanh(A_2)-1] & \text{if } I<I_*\end{cases}, \tag{7}$$

where $A_1 = -[S(z,t)+R]/L$ and $A_2 = -[S(z,t)-R]/L$ are dimensionless functions that capture the relative rate of change in light intensity and $\tanh(A_i)$ is used to model a smooth sigmoidal transition between upward and downward swimming [Fig. 1(c)]. The parameter $L$ quantifies the sensitivity of zooplankton to light stimuli: small values ($L\ll 1$ s$^{-1}$) produce sharp responses, while larger values ($L\gg 1$ s$^{-1}$) yield smoother transitions (Supplemental Material Fig. S1 [60]). The threshold parameter $R$ represents the rheobase [5,31]—the minimum rate of change in light intensity causing a response. Considering the time and length scales of our simulations, we use a value $R = 10^{-2}$ s$^{-1}$. We remark that for $R\geqslant 20$, the swimming response is strongly attenuated, resulting in near-zero vertical velocities, $w(z,t)\approx 0$. The functional $S(z,t)$ captures the local rate of change in light intensity and is defined as $S(z,t) = \partial_t[I(z,t)/I_0] + k_d u_0$, where $(k_d u_0)^{-1}$ characterizes the timescale over which the light intensity

experienced by the organism changes as it moves through the vertical light gradient.

Finally, the agent orientation, $\hat{\mathbf{p}}_i$ in Eq. (2) is modeled by the action of two processes: (i) active fluctuations following a white Gaussian noise $\boldsymbol{\xi}_R$ with zero mean, $\langle \boldsymbol{\xi}_R(t) \rangle = 0$, and delta-correlated in time, $\langle \boldsymbol{\xi}_R(t_1)\boldsymbol{\xi}_R(t_2) \rangle = D_R \delta(t_1 - t_2)$, where $D_R$ is the rotational diffusion coefficient; and (ii) a deterministic gravitational torque term [46,61], which describes the tendency of the swimmer to reorient toward the vertical direction over a characteristic timescale $\tau_G$ as illustrated in Fig. 1(b). Our modeling framework does not allow spatial overlap of organisms, meaning they need to reorient and move to avoid collisions while swimming (Methods), neglects hydrodynamic interactions between organisms, turbulence in the water column, and cell growth.

## III. RESULTS

### A. Brownian versus ABM excursions

Let us first examine the behavior of an individual organism moving according to the Langevin equations (1) and (2), which are explicitly integrated forward in time in a three-dimensional domain that is closed at the top, open at the bottom, and periodic in the lateral directions (Methods). A first consequence of light-mediated swimming is a substantial increase in vertical excursion compared to purely Brownian exploration. We illustrate this by comparing the trajectories of two self-propelled spherical agents of body length (diameter) $\sigma$: one exposed to constant darkness ($I = 0$) and the other to a day-night light cycle ($I \geqslant 0$). Their paths are shown in Fig. 2, where green and red dots mark the initial and final positions after one cycle, respectively. In darkness, the organism exhibits a noisy, wandering trajectory controlled by rotational diffusion ($D_R = 10\,\tau_G^{-1}$) and gyrotaxis, resulting in an exploration length scale $\ell_e \propto \mathcal{O}(10^1\sigma)$ and a vertical speed uniformly distributed between 0 and 1 [Fig. 2(a)]. By contrast, under a day-night light cycle, the same organism undergoes a markedly different motion [Fig. 2(b)], characterized by a long-range, back-and-forth vertical excursion on the order of $\ell_e \propto \mathcal{O}(10^3\sigma)$ and a bi-modal swimming speed distribution. These contrasting trajectories and kinematics highlight the powerful role of light and photokinesis in enhancing motility, enabling organisms to explore their environment across spatial scales far larger than those achievable through stochastic dynamics alone.

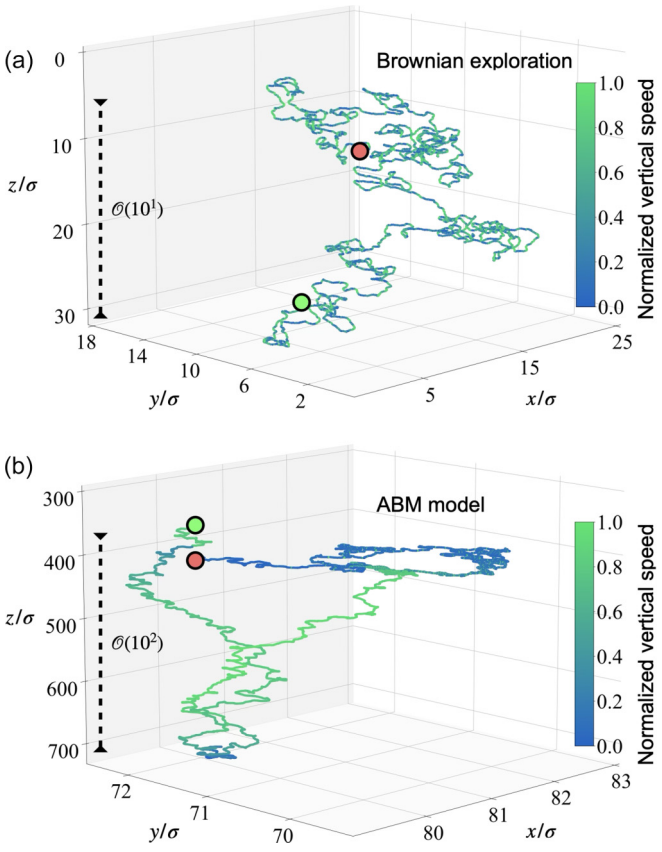



FIG. 2. Trajectories and normalized vertical swimming speed, $|w|/u_0$, for a modeled organism with photokinesis, gyrotaxis, and Brownian motion under two light regimes: (a) constant darkness over one diel cycle; (b) a day–night cycle with photokinesis active during the daytime. The green dot marks the initial position; the red dot marks the final position.

### B. Population-scale collective patterns

Upscaling the analysis to a swarm of swimming organisms reveals the emergence of population-scale dynamics. Initially, organisms are uniformly distributed in the horizontal ($x$-$y$) plane, and their vertical initial position is uniformly distributed around the nocturnal niche $z = H$ (Supplemental Material Fig. S2 [60]). Their subsequent trajectories then evolve according to the Langevin equations of motion (1) and (2). From individual trajectories, we zoom-out and reconstruct the spatiotemporal concentration field of the swarm over four diel light cycles and investigate the resulting macroscopic behavior in terms of two key parameters. The first is the organism-scale Péclet number, $\mathrm{Pe} = u_0/(D_R\sigma)$, which quantifies the ratio between active self-propulsion and rotational diffusion. For $\mathrm{Pe} < 1$, the swimmer's motion is predominantly diffusive, whereas for $\mathrm{Pe} > 1$, directional persistence dominates. The second parameter is the vertical speed ratio during the diel vertical migration, defined as $W = w_{\mathrm{down}}/w_{\mathrm{up}}$. Without loss of generality, and to reduce computational cost, we define the niche isolume as the time-dependent depth at which light intensity reaches 8% of the surface maximum, $I_* = 0.08 I_0$. Simulations are performed in a domain with depth $L_z = 4 \times 10^3\sigma$, a constant density of organisms $n = N/V = 1.25 \times 10^{-5}$, where the intensity of light in the deepest region is approximately 5% of the surface value (Supplemental Material Fig. S1 [60]). All organisms and simulations have the same characteristic self-propulsion speed $u_0$, gyrotactic reorientation timescale $\tau_G = 1$, and upward swimming speed $w_{\mathrm{up}} = 2u_0$. To explore the population-scale response, we systematically vary Pe and $W$ by tuning the rotational diffusion coefficient $D_R$ and downward swimming speed $w_{\mathrm{down}}$. These parameter ranges encompass behaviors observed across a wide variety of marine microorganisms [24,62,63]. The list of simulation parameters is provided in Supplemental Material Table S1 [60].

To quantify how individual-scale kinematic behaviors shape population-level distributions, we compute the

probability density function (PDF) $n(z)$ of the time- and horizontally averaged concentration field $C(t, \boldsymbol{x})$, which captures the statistics of the depth-time swimmers'distribution, $C_h(t, z)$ (Methods). This quantity parallels the signal of plankton commonly inferred from the acoustic backscatter measured by acoustic Doppler current profilers [64–66]. Our results reveal that variations in self-propulsion strength (Pe) and vertical-speed ratio ($W$) give rise to four distinct collective behavior, spanning broadly dispersed vertical distributions to highly concentrated, light-coherent periodic motion. Representative examples are shown in Fig. 3, and we highlight their properties next.

#### 1. Surface accumulation

This regime occurs when organisms exhibit strong orientational persistence and asymmetric motility that favors upward swimming, as illustrated in Fig. 3(a) for Pe $= 100$ and $W = 0.1$. Under these conditions, organisms actively explore the upper water column, remaining predominantly confined between the surface and the prescribed nocturnal niche depth [$z/H = 1$; Fig. 1(b)]. This behavior is quantitatively captured by the time series of the population center of mass, $\langle z(t)\rangle/H$ (with $\langle\cdot\rangle$ a time- and horizontally averaged operator, Methods), which remains consistently below one, indicating persistent residence above the nocturnal niche (see the Supplemental Material [60]). The resulting vertical distribution reflects a balance between upward dispersion and light-driven stabilization at the niche isolume $I_*$. The PDF $n(z)$ of the vertical concentration profile $C_h(t, z)$ over four day cycles [Fig. 4(a)] reveals two peaks, a primary peak near $z/H = 1$, and a secondary peak near the surface ($z/H = 0$), separated by a relatively flat intermediate region—evidence of continuous vertical movement within the upper layer (Supplemental Material Video S1 [60]).

#### 2. Shallow DVM

In this regime–characterized by high vertical motility asymmetry favoring upward motion ($W \lesssim 0.25$)—organisms accumulate at the nocturnal niche depth ($z/H = 1$) due to the lack of swimming strength to effectively keep track of the diel variation in depth ($z_*$) of $I_*$ (see Fig. S3 in the Supplemental Material [60]). As a result, the vertical concentration field $C_h(t, z)$ exhibits limited vertical mobility, constrained to shallow dives in attempt to swim toward darker waters (Fig. 3(b) and Supplemental Material Video S2 [60]). The PDF $n(z)$ [Fig. 4(b)] displays a narrowly confined peak, a thin layer with negligible vertical dispersion, indicating strong localization and minimal environmental responsiveness.

#### 3. Deep DVM

This regime represents a canonical pattern of diel vertical migration observed in natural systems. It is achieved by organisms that have well-balanced upward and downward vertical swimming capabilities, with $W \approx 1$. As an example, Fig. 3(c) (Supplemental Material Video S3 [60]) shows organisms that respond effectively to the changing light intensities, resulting in synchronized upward and downward migrations that follow the daily cycle. Under these conditions, the population center of mass exhibits only small deviations from the prescribed niche isolume, as quantified in Fig. S3 in the Supplemental Material [60]. The vertical concentration field $C_h(z, t)$ exhibits a periodic structure, reflecting coordinated population movement in phase with solar forcing. The corresponding PDF $n(z)$ [Fig. 4(c)] features a sharp peak at the nocturnal niche and an extended tail reaching into deeper waters, capturing the full amplitude of the migratory path.

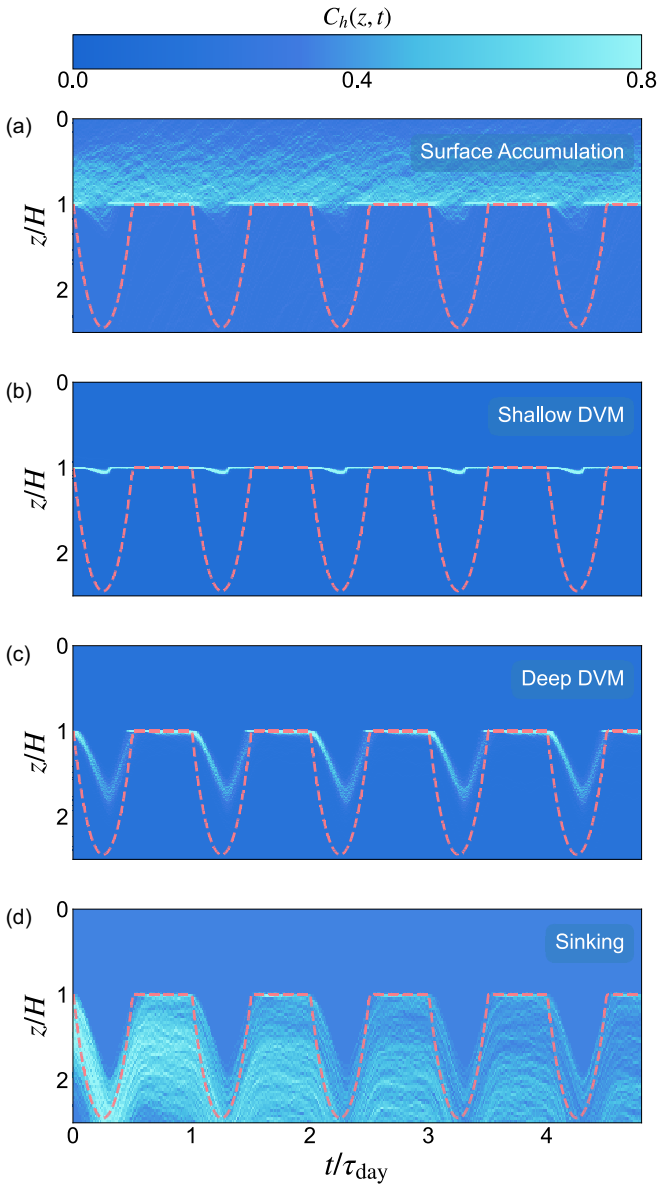



FIG. 3. Swarm collective patterns under diel light forcing. Horizontally averaged vertical concentration $C_h(z, t)$ over time highlighting distinct collective behaviors. Dashed curve displays time-dependent depth $z_*(t)/H$ of the isolume $I_*$ during daytime and nighttime $z/H = 1$. (a) *Surface accumulation* (Pe $= 100$, $W = 0.1$): swarm confined to the upper 10% of the water column. (b) *Shallow DVM* (Pe $= 0.1$, $W = 0.1$): thin layer forms at the nocturnal niche ($z/H = 1$). (c) *Deep DVM* (Pe $= 10$, $W = 0.8$): synchronized tracking of the diel isolume. (d) *Sinking* (Pe $= 10$, $W = 1.2$): gradual descent and dispersion below the niche isolume. All the regimes described are shown in Supplemental Material Video S5 [60].

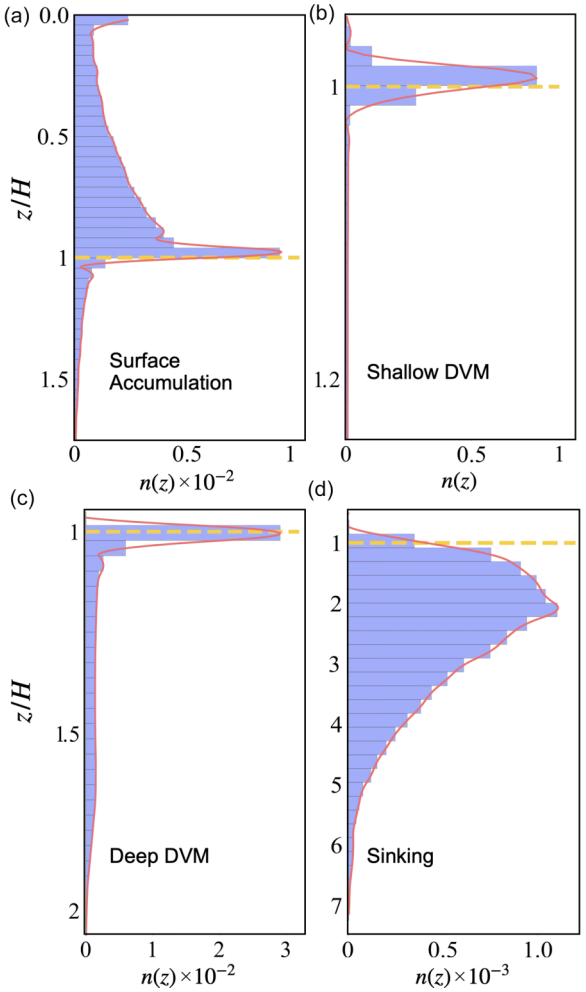



FIG. 4. Vertical distribution of organisms across regimes. Probability density distribution $n(z)$ of the time- and horizontally averaged concentration, $\langle C(\boldsymbol{x}, t)\rangle$, over a four-day cycle for representative combinations of simulation parameters, illustrating the four identified behavioral regimes. The yellow dashed line marks the nocturnal niche depth $H$, the preferred nighttime position of the organisms. The red curve shows the smoothed interpolation used to compute the normalized mean position and excess kurtosis of the distribution. Examples of: (a) *surface accumulation* (Pe $= 100$, $W = 0.1$), (b) *shallow DVM* (Pe $= 0.1$, $W = 0.1$), (c) *deep DVM* (Pe $= 10$, $W = 0.8$, and (d) *sinking* (Pe $= 10$, $W = 1.2$).

#### 4. Sinking

This regime arises when organisms remain sensitive to light cues but are unable to track the upward motion of the niche isolume, resulting in a net downward drift (see Fig. S3 in the Supplemental Material [60]). It occurs when motility is persistent but vertically biased, as in the case illustrated in Fig. 3(d) (Supplemental Material Video S4 [60]) for Pe $= 10$ and $W = 1.2$. The elevated downward swimming speed overwhelms photokinetic reorientation, causing organisms concentration $C_h(z, t)$ to sink progressively over time. Although they respond to diel light cycles, the inability to rapidly reverse direction prevents full vertical recovery. The PDF $n(z)$ [Fig. 5(d)] reflects this behavior, showing a broad, uniform distribution deeper than the nocturnal niche.

### C. Mapping and bounding collective patterns

To classify the four behavioral regimes across the parameter space (Pe, $W$), we studied the statistical properties of the PDF $n(z)$ for all simulation cases listed in Supplemental Material Table S1 [60] (examples shown in Fig. 4). From each PDF, we computed two statistical descriptors: the normalized average, $\mu/L_z$, representing the mean vertical position of the population, and the excess kurtosis, $\alpha$, which quantifies the peakedness and tail weight, thereby reflecting the extent of vertical spread. These metrics are mapped over the (Pe, $W$) domain in Figs. 5(a) and 5(b) (Methods).

#### 1. Swarm's center of mass

The normalized mean vertical position, $\mu/L_z$, captures how the population's center of mass shifts across the parameter space (Pe, $W$), as shown in Fig. 5(a). Low values of $\mu/L_z$ (blue) indicate *Surface Accumulation* (SA), while high values (red) reflect populations distributed in deeper regions. The isolume zone, where light intensity reaches 8% of that at the surface, corresponds to $0.1 \leqslant \mu/L_z \leqslant 0.25$ (or $1 \leqslant z/H \leqslant 2.5$ as showin in Fig. 3). Values below this range ($\mu/L_z < 0.1$) reflect accumulation in high-light surface layers, typical of the SA regime, whereas values above 0.25 correspond to the *Sinking* regime, with the population concentrated in deeper, darker waters [Fig. 4(d)].

#### 2. Swarm's vertical distribution

The kurtosis $\alpha$ characterizes the shape of the vertical distribution. Its variation through the parameter space (Pe, $W$) [Fig. 5(b)] shows that high values ($\alpha \geqslant 3$) mark sharply peaked profiles, indicating trapping near the nocturnal niche depth. Intermediate values ($0 < \alpha < 3$) correspond to peaked distributions with extended tails, typical of SA and deep DVM. Negative or near-zero values ($\alpha \leqslant 0$) indicate broad, flat distributions with long tails, consistent with *Sinking* or deep diffusion into darker waters.

### D. Stochastic versus directed motility

Our results show that when Pe $< 1$, where stochastic (Brownian) reorientation dominates over directed swimming, collective dynamics are largely insensitive to Pe but strongly shaped by the vertical velocity ratio $W = w_{\text{down}}/w_{\text{up}}$. As $W$ increases, three distinct behavioral regimes emerge: *shallow DVM*, *deep DVM*, and *sinking* [Figs. 5(a) and 5(b)]. In the absence of light cues, the orientation distribution of gyrotactic swimmers is governed by the Fokker–Planck equation [42],where azimuthal orientations are uniformly distributed and gyrotactic alignment leads to a polar orientation antiparallel to gravity, characterized by a nonzero mean vertical polarization $\langle \hat{\mathbf{p}} \cdot \hat{\mathbf{k}} \rangle = \langle p_z \rangle = \coth(\lambda) - 1/\lambda$. Here, $\lambda = \text{Pe}\,[\sigma/(\tau_G u_0)]$ is a dimensionless parameter, proportional to Pe, comparing the gyrotactic reorientation timescale $\tau_G$ to the persistence time of the swimmer. We compute $\langle p_z \rangle$ as a function of Pe for several values of $\tau_G$ ($10^{-2}$ to $10^{1}$), shown as color-coded curves from blue to green in Fig. 5(c). For $\tau_G = 1$ (pink curve), gyrotaxis dominates at Pe $> 10$, causing swimmers to align upward against gravity. This alignment supports the emergence of the *surface accumulation* regime

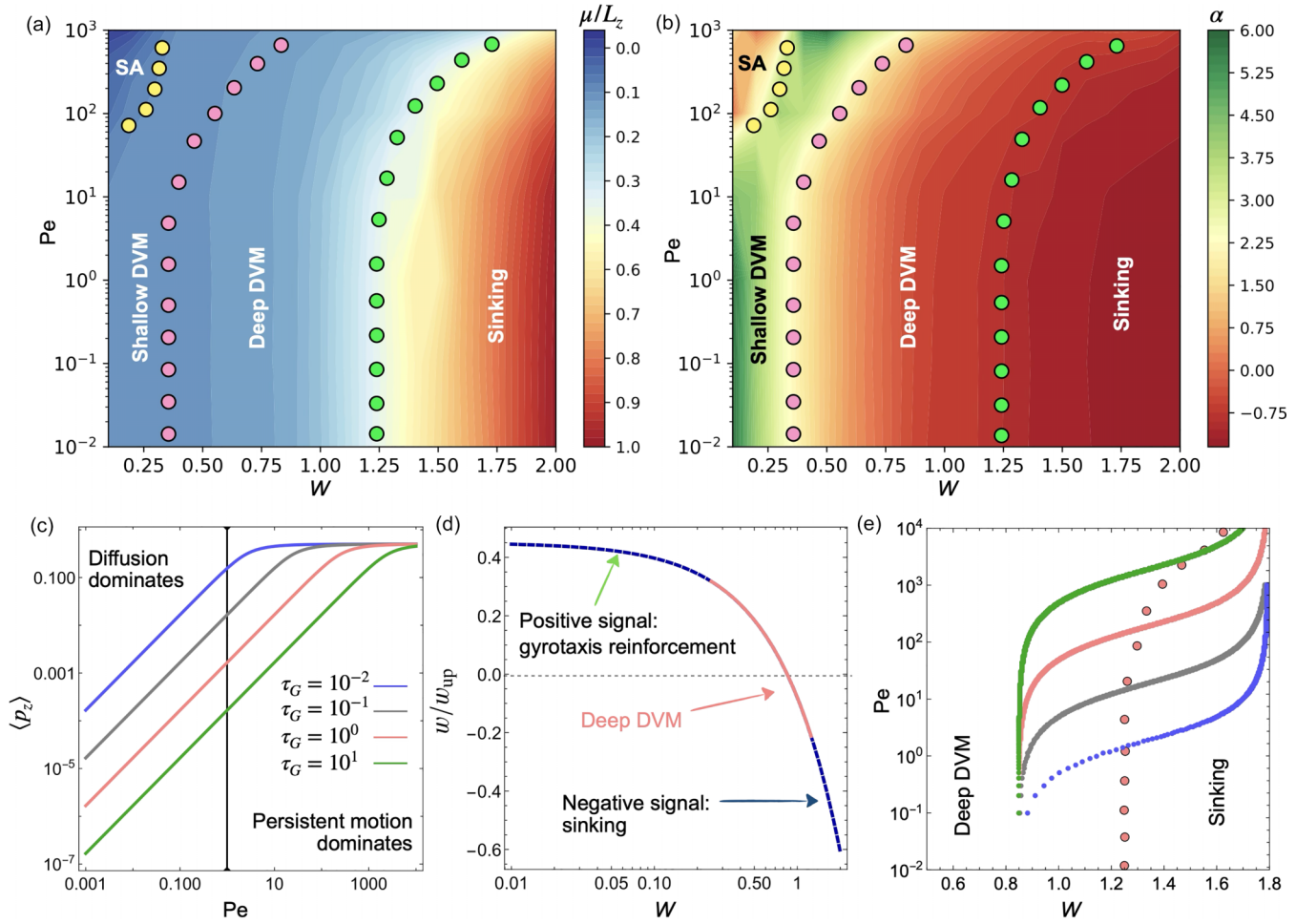



FIG. 5. Phase diagram and swimming regimes of organisms. (a), (b) Phase diagrams of the normalized average $\mu/L_z$ and the excess kurtosis $\alpha$ of the time-averaged vertical distribution, over the different simulations, mapped as functions of the Péclet number Pe and the vertical swimming asymmetry ratio $W$. Colored dots delineate regime boundaries: yellow indicates the transition from *surface accumulation* to trapping; pink marks the boundary between trapping and diel vertical migration; green defines the transition to the *Sinking* regime. (c) Mean vertical orientation $\langle p \rangle$ as a function of Pe and varying gyrotactic reorientation timescale $\tau_G$: blue ($10^{-2}$), gray ($10^{-1}$), pink ($10^{0}$), and green ($10^{1}$). The pink curve represents the configuration used in the present model. (d) Instantaneous ratio of vertical swimming speed to upward velocity, $w/w_{\mathrm{up}}$, evaluated at depth $z = H$ and time $t$, shown as a function of $W$. Green arrow indicates the conditions under which diel vertical migration emerges; the red arrow marks the transition to *sinking*. (e) Critical value of $W$ (Pe) at which the vertical velocity statistically becomes zero ($w = 0$), for different values of $\tau_G$: blue ($10^{-2}$), gray ($10^{-1}$), pink ($10^{0}$), and green ($10^{1}$).

within a narrow range of low-$W$ [Fig. 3(b)]. More broadly, when $W < 1$, upward swimming enhances gyrotactic alignment, promoting both *surface accumulation* and *shallow DVM* dynamics [Figs. 3(a) and 3(b)]. In contrast, we expect this regime to vanish in the absence of gyrotaxis.

For $W > 1$, downward swimming dominates, driving organisms to dive deeper into the water column. At low-Pe ($<1$), the stochastic reorientation overwhelms directional swimming, resulting in a progressive *Sinking* [Fig. 3(d)]. Conversely, at high-Pe ($>100$), strong directional persistence allows organisms to maintain alignment with the target isolume despite the downward bias, thereby sustaining *deep DVM*.

Intriguingly, our results show that *deep DVM* can emerge from a wide range of Pe and $W$ values. This raises a fundamental question: How can such behavior arise from simple, local motility rules? Clues are inferred from examining how the swimming strategy modulates the organism's vertical velocity as a function of the velocity ratio $W$,

$$w(z,t)/w_{\mathrm{up}} = 1 + \frac{\tanh(A_1) + \tanh(A_2)}{2} - \frac{W}{2}, \qquad (8)$$

displayed in Fig. 5(d). This relationship reveals a positive feedback mechanism: for $W < 0.1$, the vertical velocity is enhanced, favoring upward movement and increasing the likelihood of *surface accumulation* and *shallow DVM*. As $W$ increases, the net vertical velocity decreases, eventually becoming negative, promoting downward drifting. This transition suppresses directed migration and amplifies diffusion-dominated behavior, reinforcing the *sinking* of organisms

From Fig. 5, we identify the *deep DVM* regime within the interval $0.3 \leqslant W \leqslant 1.25$ at low-Pe ($\lesssim 1$), corresponding to a transition zone where the light signal induces a

switch from upward to downward vertical swimming. In this region, the magnitude of the vertical velocity satisfies $|w|/w_{\mathrm{up}} \sim 0.4$. This subtle balance reveals the organism's capacity to regulate upward and downward swimming, which in turn may involve the ability to perform sharp reorientations. Such behavior has been observed in phytoplankton communities like Heterosigma *akashiwo* [52,67], which exhibit brief transitions where organisms adjust their orientation to track changes in the niche isolume depth. That is, they can orient upward while downward swimming or orient downward while swimming toward the surface (Supplemental Material Fig. S4 [60]).

To understand this mechanism, let us analyze the Langevine equation of motion Eq. (1). If we neglect swimmer-swimmer hard-core interactions in Eq. (1), the above behavior can be interpreted as a swimmer that suspends its vertical motion, i.e., $v_z = \dot{\mathbf{r}} \cdot \hat{\mathbf{k}} = 0$. Taking the average over all possible swimmer's orientation, $\langle p_z \rangle = \coth(\lambda) - 1/\lambda$, Eq. (1) yields the following approximation for the vertical velocity ratio:

$$W \approx \left\{ 1 + 2\frac{u_0}{w_{\mathrm{up}}} \left[ \coth(\lambda) - \frac{1}{2\lambda} \right] \right\}. \tag{9}$$

This functional relationship for $W$ is plotted in terms of Pe in Fig. 5(e) for different gyrotactic timescales $\tau_G = 10^{-2}$, $10^{-1}$, $10^{0}$, $10^{1}$, represented by blue to green dashed lines, respectively. We observe that the condition $w = 0$ defines a region in which DVM can emerge. Interestingly, the smallest value of $W$ for which this condition is satisfied is $W = 1$, which appears independent of the gyrotactic timescale $\tau_G$; this limit is shifted slightly to the right in our numerical results, shown as a dotted pink line. This sets a boundary for the *sinking* regime, with large $\tau_G$ (strong gyrotactic reorientation) shrinking the DVM region (see blue dashed curve) to smaller Péclet numbers.

## IV. DISCUSSION

DVM is the largest synchronized movement of biomass on the planet, playing a pivotal role in aquatic food webs and biogeochemical cycling in oceans and lakes [2,5,68]. While classical continuum models have captured its large-scale patterns [31,59,69], laboratory studies have revealed complex organismal mechanisms that underpin this collective phenomenon, their capacity to swim long distances and enhance mixing in aquatic systems [20,26,30,70,71].

Here, we introduce an ABM framework and show how macroscale DVM patterns can arise from simple, local behavioral rules in photokinetic swimmers navigating a dynamic light field. Each organism is modeled as an active gyrotactic Brownian sphere that adjusts its swimming in response to local light intensity and gradients. Remarkably, we find that population-scale dynamics are governed by just two dimensionless parameters: the Péclet number (Pe), representing the persistence of directed motion relative to rotational diffusion, and the vertical velocity ratio ($W = w_{\mathrm{down}}/w_{\mathrm{up}}$), capturing asymmetry in photokinetic response across a critical isolume value $I_*$.

Brownian dynamics simulations (Methods) across a broad $(\mathrm{Pe}, W)$ parameter space reveal four distinct collective regimes: (i) *surface accumulation*, where organisms remain near the upper water column; (ii) *shallow DVM*, with tightly confined diel vertical excursions; (iii) *deep DVM*, characterized by pronounced excursions synchronized with daytime changes in isolume depth; and (iv) *sinking*, where populations drift irreversibly into deeper waters. These regimes emerge from nonlinear interactions among rotational noise, gyrotactic alignment, and light-sensitive speed modulation.

In the *surface accumulation* regime, swimmers disperse between the free-surface and the nocturnal niche, making short, asynchronous excursions during the daytime. This accumulation results from the reinforcement of the gyrotactic organism's response and swimming strategy at small $W$, combined with the nonpenetration boundary condition imposed at the free surface. Such behavior is observed in phytoplankton like dinoflagellate species [72] and small zooplankton rotifers like *Keratella cochlearis* [29,73], which typically remain within the upper photic zone. Their confinement is often attributed to weak swimming ability and enhanced diffusion from surface-layer turbulence [74], where turbulence disrupts gyrotactic shear trapping and promotes vertical dispersion [75,76]. In contrast, *shallow DVM* occurs across all the explored Péclet numbers when the vertical velocity ratio satisfies $W \lesssim 0.25$. Organisms in this regime form sharply localized distributions and perform synchronized, yet shallow, dives during daylight hours. This behavior resembles the gyrotactic trapping observed in laminar shear flows in the absence of external directional cues [28,67,75,77,78], as documented for species such as the dinoflagellate *Akashiwo sanguinea* [52,79].

The *deep DVM* regime represents the most widespread form of collective plankton migration in both oceans and lakes [2,5,17–19,66]. While previous studies have relied on one-dimensional continuum models—among which the most comprehensive incorporate predator–prey dynamics and biogeochemical stimuli [2,5,31,80]—our work presents the first fully three-dimensional agent-based framework that reproduces canonical DVM behavior directly from organism-scale motility rules. We find that *deep DVM* consistently emerges when upward and downward swimming speeds are balanced, with vertical velocity ratios clustering around $W \approx 1$. This balance yields robust diel excursions across a broad range of Péclet numbers (Pe), as individuals synchronize their directional switching with the daily movement of the isolume. Such behavior mirrors that observed in laboratory experiments for phytoplankton species such as *H. akashiwo* [67] and "model" zooplankton species such as *Daphnia magna* [15,20,81] and *Artemia Salina* [26,82,83]. Beyond this delicate balance lies the *sinking* regime, which marks a clear boundary in the DVM phase space [Figs. 5(a) and 5(b)]. The sinking regime identified here does not represent a passive or permanent sinking state, but a transient dynamical response to a strong downward swimming bias while organisms still perceive a light gradient that decays exponentially with depth. For $W > 1$, photokinetic asymmetry overwhelms orientational control, leading to persistent downward motion and loss of isolume tracking across all Pe values; once the light signal becomes undetectable, the dynamics cross over to unbiased stochastic swimming.

Our study sheds light on how simple, organism-encoded physiology and swimming strategy can give rise to collective macroscale patterns in aquatic ecosystems. By bridging individual photokinetic and gyrotactic behaviors with population-level dynamics, this framework offers a mechanistic foundation to probe biological processes critical to oceans and lakes functioning—from carbon sequestration via the biological pump to nutrient redistribution [2,3,24,84], harmful algal blooms [67], and the ecological consequences of climate change [1,3,5,80]. Beyond its ecological insights, the model also provides a predictive tool to explore how light-responsive active matter systems self-organize across environmental gradients. Future directions could integrate depth-dependent turbulence fluctuations that can interact with the swarm and the organism itself [25,30,85,86], hydrodynamic coupling [17,51,71,87,88], multispecies systems [66], and adaptive behaviors under variable light regimes [19], broadening the model's representation of processes and systems.

## V. METHODS

### A. Dimensionless parameters and simulations

We employed standard Brownian dynamics methods (explicit Euler integration) to numerically solve the governing equations (1) and (2) for a population of $N$ (Supplemental Material Table S1 [60]) organisms moving in a three-dimensional space of size $L_x \times L_y \times L_z$. Periodic boundary conditions were applied in the $x$-$y$ plane, while a Dirichlet condition $w(z=0)=0$ was imposed at the free surface and an open boundary was set at the bottom $z=L_z$. To handle periodic boundary conditions, we used the minimum-image convention to compute hard-core interactions near the borders. To reduce redundant computations, we evaluated pairwise interactions exploiting symmetry (i.e., considering only $j>i$) and assigned each particle a Verlet neighbor list. The initial distribution of particles followed a Gaussian profile centered at the nocturnal isolume depth $H$, while particle orientations were initially drawn from a uniform distribution with zero mean and unit standard deviation. Under these conditions, at each time step of size $\Delta t$, the noise generated via Box-Muller transform was coupled to gyrotaxis, and particle positions were updated according to self-propulsion, pairwise interactions, and the swimming strategy, using explicit Euler integration over a total of $T$ iterations (Supplemental Material Table S1 [60]).

To generalize the system and reduce the number of free parameters, we set $\tau_G$ [46] and the particle diameter $\sigma$, as the time and length units of our problem, respectively. Environmental factors introduced a new set of parameters, which we kept fixed throughout the numerical simulations: the bulk coefficient of light spatial attenuation $\kappa_d$, the light intensity $I_0$, and the day timescale $\tau_{\text{day}}$.

We are interested in studying the effects on collective motion arising from individual response to the light signal, here accomplished by the swimming strategy, self-propulsion, and diffusive motion. Therefore we define two dimensionless parameters: the Péclet number $\text{Pe}=u_0/(D_R\,\sigma)$ which compares advective to diffusive timescales, and the vertical velocity ratio $W=w_{\text{down}}/w_{\text{up}}$, which captures the imbalance in the vertical swimming during the photokinetic response.

We performed 120 simulations varying the pair $(\text{Pe}, W)$, through the parameters $D_R$ and $w_{\text{down}}$. To account for a mixed phenotype collection of organisms [19,24,63], we set a value $w_{\text{down}}$ and we assigned to each organism a given downward velocity generated from a Poisson distribution, $P(X=k)=\Lambda^k e^{-\Lambda}/k!$, with $\Lambda=w_{\text{down}}$ representing the mean value of the distribution. Finally, we perform a statistical analysis of the simulations, which is detailed in the Supplemental Material [60].

### B. Operators and observables

We utilize different operators and we estimate different physical quantities. The horizontal average of the organisms concentration field $C(\boldsymbol{x},t)$—illustrated in Fig. 3—is determined as

$$C_h(z,t)=\frac{1}{A_{xy}}\int_0^{L_y}\int_0^{L_x} C(\boldsymbol{x},t)\,dx\,dy, \tag{10}$$

where $A_{xy}=L_x\times L_y$ is the area of the horizontal domain $x$-$y$. The time- and horizontally averaged quantity of a three-dimensional scalar field $f(\boldsymbol{x},t)$, like the organism's vertical velocity $w(\boldsymbol{x},t)$ or concentration $c(\boldsymbol{x},t)$ is denoted as

$$\langle f\rangle=\frac{1}{\Delta T}\int_{t_i}^{t_f}\frac{1}{A_{xy}}\int_0^{L_y}\int_0^{L_x} f(\boldsymbol{x},t)\,dx\,dy\,dt, \tag{11}$$

$\Delta T=t_f-t_i$ is the time window over which the time-average is performed. For instance, the time- and horizontally averaged organisms concentration, analyzed in Fig. 4, is denoted as $n(z)=\langle C\rangle$.

### C. Probability density function and statistics

We construct a histogram from the time-averaged vertical position of the organisms, shown as purple bins in Fig. 4 (see details in the Supplemental Material [60]). From this histogram, we compute the corresponding PDF using NumPy, SciPy, and MatPlotLib in Python. This fit is plotted as a red curve in Fig. 4.

To construct the colormap in Fig. 5, we compute the PDF for each simulation corresponding to a given pair of parameters $(\text{Pe}, W)$, and analyze its statistical properties—specifically, the mean $\mu$ and kurtosis $\alpha$. We then plot the average values of $\mu$ and $\alpha$ over the set of simulations and interpolate these quantities to generate the phase diagram.

## ACKNOWLEDGMENTS

F.G.-L. and J.M. were supported by Fondecyt Iniciación Grant No. 11220683. This research was partially supported by the supercomputing infrastructure of the NLHPC (CCSS210001). D.N. and H.N.U. were supported by start-up grant University of Pennsylvania. This project was supported by the PURM Program 2022 University of Pennsylvania: "Escaping from light—A circadian migration of active matter in aquatic systems." Last, we thank the anonymous reviewers for their thoughtful and constructive feedback.

F.G.-L. and H.N.U. conceived the problem and the modeling framework. D.N. developed the swimming strategy model. J.M. and P.M. developed the code. J.M. performed the

simulations. All authors analyzed the results and reviewed the manuscript.

The authors declare no competing interests.

## DATA AVAILABILITY

The data that support the findings of this article are openly available [89].


[1] G. C. Hays, A review of the adaptive significance and ecosystem consequences of zooplankton diel vertical migrations, Hydrobiologia **503**, 163 (2003).

[2] D. Bianchi, C. Stock, E. D. Galbraith, and J. L. Sarmiento, Diel vertical migration: Ecological controls and impacts on the biological pump in a one-dimensional ocean model, Global Biogeochem. Cycles **27**, 478 (2013).

[3] D. K. Steinberg and M. R. Landry, Zooplankton and the ocean carbon cycle, Annu. Rev. Mar. Sci. **9**, 413 (2017).

[4] K. M. Archibald, D. A. Siegel, and S. C. Doney, Modeling the impact of zooplankton diel vertical migration on the carbon export flux of the biological pump, Global Biogeochem. Cycles **33**, 181 (2019).

[5] J. Ringelberg, *Diel Vertical Migration of Zooplankton in Lakes and Oceans: Causal Explanations and Adaptive Significance* (Springer, Berlin, 2010).

[6] K. Bandara, Ø. Varpe, L. Wijewardene, V. Tverberg, and K. Eiane, Two hundred years of zooplankton vertical migration research, Biol. Rev. **96**, 1547 (2021).

[7] Z. M. Gliwicz, Predation and the evolution of vertical migration in zooplankton, Nature (London) **320**, 746 (1986).

[8] S. M. Bollens and B. Frost, Predator-induced diet vertical migration in a planktonic copepod, J. Plankton Res. **11**, 1047 (1989).

[9] W. Lampert, The adaptive significance of diel vertical migration of zooplankton, Funct. Ecol. **3**, 21 (1989).

[10] W. E. Neill, Induced vertical migration in copepods as a defence against invertebrate predation, Nature (London) **345**, 524 (1990).

[11] T. B. Kelly, P. C. Davison, R. Goericke, M. R. Landry, M. D. Ohman, and M. R. Stukel, The importance of mesozooplankton diel vertical migration for sustaining a mesopelagic food web, Front. Mar. Sci. **6**, 508 (2019).

[12] M. Ludvigsen, J. Berge, M. Geoffroy, J. H. Cohen, P. R. De La Torre, S. M. Nornes, H. Singh, A. J. Sørensen, M. Daase, and G. Johnsen, Use of an autonomous surface vehicle reveals small-scale diel vertical migrations of zooplankton and susceptibility to light pollution under low solar irradiance, Sci. Adv. **4**, eaap9887 (2018).

[13] T. Fenchel, Microbial behavior in a heterogeneous world, Science **296**, 1068 (2002).

[14] G. Jékely, Evolution of phototaxis, Phil. Trans. R. Soc. B **364**, 2795 (2009).

[15] C. Noss and A. Lorke, Direct observation of biomixing by vertically migrating zooplankton, Limnol. Oceanogr. **59**, 724 (2014).

[16] C. Dean, A. Soloviev, A. Hirons, T. Frank, and J. Wood, Biomixing due to diel vertical migrations of zooplankton: Comparison of computational fluid dynamics model with observations, Ocean Modell. **98**, 51 (2016).

[17] R. Ouillon, I. Houghton, J. Dabiri, and E. Meiburg, Active swimmers interacting with stratified fluids during collective vertical migration, J. Fluid Mech. **902**, A23 (2020).

[18] N. S. Häfker, S. Connan-McGinty, L. Hobbs, D. McKee, J. H. Cohen, and K. S. Last, Animal behavior is central in shaping the realized diel light niche, Commun. Biol. **5**, 562 (2022).

[19] N. S. Häfker, G. Andreatta, A. Manzotti, A. Falciatore, F. Raible, and K. Tessmar-Raible, Rhythms and clocks in marine organisms, Annu. Rev. Mar. Sci. **15**, 509 (2023).

[20] D. Noto and H. N. Ulloa, Simple tracking of occluded self-propelled organisms, Meas. Sci. Technol. **35**, 035705 (2024).

[21] T. J. Pedley and J. O. Kessler, Hydrodynamic phenomena in suspensions of swimming microorganisms, Annu. Rev. Fluid Mech. **24**, 313 (1992).

[22] W. M. Durham and R. Stocker, Thin phytoplankton layers: Characteristics, mechanisms, and consequences, Annu. Rev. Mar. Sci. **4**, 177 (2012).

[23] B. Chen, E. Masunaga, S. L. Smith, and H. Yamazaki, Diel vertical migration promotes zooplankton horizontal patchiness, J. Oceanogr. **77**, 123 (2021).

[24] A. Sengupta, F. Carrara, and R. Stocker, Phytoplankton can actively diversify their migration strategy in response to turbulent cues, Nature (London) **543**, 555 (2017).

[25] F.-G. Michalec, I. Fouxon, S. Souissi, and M. Holzner, Zooplankton can actively adjust their motility to turbulent flow, Proc. Natl. Acad. Sci. USA **114**, E11199 (2017).

[26] I. A. Houghton, J. R. Koseff, S. G. Monismith, and J. O. Dabiri, Vertically migrating swimmers generate aggregation-scale eddies in a stratified column, Nature (London) **556**, 497 (2018).

[27] M. A. Bees, Advances in bioconvection, Annu. Rev. Fluid Mech. **52**, 449 (2020).

[28] B. Wang, W. Jiang, G. Chen, L. Tao, and Z. Li, Vertical distribution and longitudinal dispersion of gyrotactic microorganisms in a horizontal plane poiseuille flow, Phys. Rev. Fluids **6**, 054502 (2021).

[29] M. Perga, M. Syarki, N. Kalinkina, and D. Bouffard, A rotiferan version of the punishment of sisyphus? Ecology **101**, e02934 (2020).

[30] M. H. DiBenedetto, R. Monthiller, C. Eloy, and L. S. Mullineaux, Plankton active response to turbulence enables efficient transport, J. Exp. Biol. **228**, jeb251123 (2025).

[31] S. A. Richards, H. P. Possingham, and J. Noye, Diel vertical migration: Modelling light-mediated mechanisms, J. Plankton Res. **18**, 2199 (1996).

[32] B.-P. Han and M. Straškraba, Modeling patterns of zooplankton diel vertical migration, J. Plankton Res. **20**, 1463 (1998).

[33] R. Ji and P. J. Franks, Vertical migration of dinoflagellates: Model analysis of strategies, growth, and vertical distribution patterns, Mar. Ecol. Prog. Ser. **344**, 49 (2007).

[34] N. T. Ouellette, A physics perspective on collective animal behavior, Phys. Biol. **19**, 021004 (2022).

[35] C. Countryman, D. Steinberg, and A. Burd, Modelling the effects of copepod diel vertical migration and community structure on ocean carbon flux using an agent-based model, Ecol. Modell. **470**, 110003 (2022).

[36] C. Huang, F. Ling, and E. Kanso, Collective phase transitions in confined fish schools, Proc. Natl. Acad. Sci. USA **121**, e2406293121 (2024).
[37] H. Hang, C. Huang, A. Barnett, and E. Kanso, Self-reorganization and information transfer in massive schools of fish, arXiv:2505.05822.
[38] T. Huang, C. Yu, K. Zhang, X. Liu, J. Zhen, and L. Wang, Complex pattern dynamics and synchronization in a coupled spatiotemporal plankton system with zooplankton vertical migration, Chaos, Solitons Fractals **175**, 114063 (2023).
[39] C. Williams and M. Bees, Photo-gyrotactic bioconvection, J. Fluid Mech. **678**, 41 (2011).
[40] M. A. Bees and N. A. Hill, Linear bioconvection in a suspension of chemotactic algae, J. Math. Biol. **36**, 269 (1998).
[41] P. A. Jumars, J. H. Trowbridge, E. Boss, and L. Karp-Boss, Turbulence-plankton interactions: A new cartoon, Marine Ecol. **30**, 133 (2009).
[42] J. O. Kessler, Individual and collective fluid dynamics of swimming cells, J. Fluid Mech. **173**, 191 (1986).
[43] J. Arrieta, M. Polin, R. Saleta-Piersanti, and I. Tuval, Light control of localized photobioconvection, Phys. Rev. Lett. **123**, 158101 (2019).
[44] A. Javadi, J. Arrieta, I. Tuval, and M. Polin, Photobioconvection: Towards light control of flows in active suspensions, Philos. Trans. R. Soc. A **378**, 20190523 (2020).
[45] R. Vincent and N. Hill, Bioconvection in a suspension of phototactic algae, J. Fluid Mech. **327**, 343 (1996).
[46] T. Pedley and J. O. Kessler, A new continuum model for suspensions of gyrotactic micro-organisms, J. Fluid Mech. **212**, 155 (1990).
[47] R. N. Bearon, D. Grunbaum, and R. A. Cattolico, Relating cell-level swimming behaviors to vertical population distributions in Heterosigma akashiwo (raphidophyceae), a harmful alga, Limnol. Oceanogr. **49**, 607 (2004).
[48] K. Son, J. S. Guasto, and R. Stocker, Bacteria can exploit a flagellar buckling instability to change direction, Nat. Phys. **9**, 494 (2013).
[49] K. C. Leptos, M. Chioccioli, S. Furlan, A. I. Pesci, and R. E. Goldstein, Phototaxis of chlamydomonas arises from a tuned adaptive photoresponse shared with multicellular volvocine green algae, Phys. Rev. E **107**, 014404 (2023).
[50] J. Dervaux, M. Capellazzi Resta, and P. Brunet, Light-controlled flows in active fluids, Nat. Phys. **13**, 306 (2017).
[51] R. Monthiller, A. Loisy, Mimi A. R. Koehl, B. Favier, and C. Eloy, Surfing on turbulence: A strategy for planktonic navigation, Phys. Rev. Lett. **129**, 064502 (2022).
[52] R. Schuech and S. Menden-Deuer, Going ballistic in the plankton: Anisotropic swimming behavior of marine protists, Limnol. Oceanogr.: Fluids Environ. **4**, 1 (2014).
[53] K. Sherman and K. A. Honey, Vertical movements of zooplankton during a solar eclipse, Nature (London) **227**, 1156 (1970).
[54] K. S. Last, L. Hobbs, J. Berge, A. S. Brierley, and F. Cottier, Moonlight drives ocean-scale mass vertical migration of zooplankton during the arctic winter, Curr. Biol. **26**, 244 (2016).
[55] N. Desai and A. M. Ardekani, Modeling of active swimmer suspensions and their interactions with the environment, Soft Matter **13**, 6033 (2017).
[56] T. Ishikawa, K. Sato, T. Omori, and K. Yoshimura, Physics of microbial taxis and behaviours in response to various physical stimuli, Philos. Trans. R. Soc. A **383**, 20240264 (2025).
[57] J. C. Prairie, K. R. Sutherland, K. J. Nickols, and A. M. Kaltenberg, Biophysical interactions in the plankton: A cross-scale review, Limnol. Oceanogr.: Fluids Environ. **2**, 121 (2012).
[58] E. Widder, S. Johnsen, S. Bernstein, J. Case, and D. Neilson, Thin layers of bioluminescent copepods found at density discontinuities in the water column, Marine Biol. **134**, 429 (1999).
[59] D. Bianchi and K. Mislan, Global patterns of diel vertical migration times and velocities from acoustic data, Limnol. Oceanogr. **61**, 353 (2016).
[60] See Supplemental Material at http://link.aps.org/supplemental/10.1103/b3m3-2ffz for additional information supporting our modeling approach and parameters, figures, and videos.
[61] G. J. Thorn and R. N. Bearon, Transport of spherical gyrotactic organisms in general three-dimensional flow fields, Phys. Fluids **22**, 041902 (2010).
[62] V. Vladimirov, M. Wu, T. Pedley, P. Denissenko, and S. Zakhidova, Measurement of cell velocity distributions in populations of motile algae, J. Exp. Biol. **207**, 1203 (2004).
[63] D. Krishnamurthy, H. Li, F. Benoit du Rey, P. Cambournac, A. G. Larson, E. Li, and M. Prakash, Scale-free vertical tracking microscopy, Nat. Methods **17**, 1040 (2020).
[64] A. Lorke, D. F. McGinnis, P. Spaak, and A. Wüest, Acoustic observations of zooplankton in lakes using a doppler current profiler, Freshwater Biol. **49**, 1280 (2004).
[65] H. R. Cheslack, Diel vertical migration and frontal variability of acoustic backscatter in the Balearic Sea, Ph.D. thesis, Massachusetts Institute of Technology, 2023.
[66] V. Piton, R. Reiss, U. Lemmin, O. Anneville, G. Many, J. Keller, V. Kindschi, H. K. Wynn, S. Rasconi, L. Laine, *et al.*, Identifying and quantifying unexpected deep zooplankton diel vertical migration in a large deep lake, Limnol. Oceanogr. **70**, 259 (2025).
[67] L. Zeng, W. Jiang, and T. J. Pedley, Sharp turns and gyrotaxis modulate surface accumulation of microorganisms, Proc. Natl. Acad. Sci. USA **119**, e2206738119 (2022).
[68] D. Bianchi, E. D. Galbraith, D. A. Carozza, K. Mislan, and C. A. Stock, Intensification of open-ocean oxygen depletion by vertically migrating animals, Nat. Geosci. **6**, 545 (2013).
[69] V. Andersen and P. Nival, A model of the diel vertical migration of zooplankton based on euphausiids, J. Mar. Res. **49**, 153 (1991).
[70] C. Noss and A. Lorke, Zooplankton induced currents and fluxes in stratified waters, Water Quality Res. J. Canada **47**, 276 (2012).
[71] N. Mohebbi, J. Hwang, M. K. Fu, and J. O. Dabiri, Measurements and modelling of induced flow in collective vertical migration, J. Fluid Mech. **1001**, A50 (2024).
[72] B. Zheng, A. J. Lucas, P. J. Franks, T. L. Schlosser, C. R. Anderson, U. Send, K. Davis, A. D. Barton, and H. M. Sosik, Dinoflagellate vertical migration fuels an intense red tide, Proc. Natl. Acad. Sci. **120**, e2304590120 (2023).
[73] U. Obertegger, G. Flaim, and R. Sommaruga, Multifactorial nature of rotifer water layer preferences in an oligotrophic lake, J. Plankton Res. **30**, 633 (2008).
[74] F. De Lillo, M. Cencini, W. M. Durham, M. Barry, R. Stocker, E. Climent, and G. Boffetta, Turbulent fluid acceleration

generates clusters of gyrotactic microorganisms, Phys. Rev. Lett. **112**, 044502 (2014).

[75] G. Li, Z. Gong, W. Jiang, J. Zhan, B. Wang, X. Fu, M. Xu, and Z. Wu, Environmental transport of gyrotactic microorganisms in an open-channel flow, Water Resour. Res. **59**, e2022WR033229 (2023).

[76] Z. Wu, L. Zeng, G. Li, Z. Gong, J. Zhan, W. Jiang, M. Xu, and X. Fu, Onset for active swimming of microorganisms to shape their transport in turbulent open channel flows, Water Resour. Res. **60**, e2024WR037586 (2024).

[77] B. Wang, W. Jiang, and G. Chen, Gyrotactic trapping of microswimmers in simple shear flows: A study directly from the fundamental smoluchowski equation, J. Fluid Mech. **939**, A37 (2022).

[78] M. S. Hoecker-Martínez and W. D. Smyth, Trapping of gyrotactic organisms in an unstable shear layer, Cont. Shelf Res. **36**, 8 (2012).

[79] J. M. Sullivan, P. L. Donaghay, and J. E. Rines, Coastal thin layer dynamics: Consequences to biology and optics, Cont. Shelf Res. **30**, 50 (2010).

[80] L. Ratnarajah, R. Abu-Alhaija, A. Atkinson, S. Batten, N. J. Bax, K. S. Bernard, G. Canonico, A. Cornils, J. D. Everett, M. Grigoratou, *et al.*, Monitoring and modelling marine zooplankton in a changing climate, Nat. Commun. **14**, 564 (2023).

[81] S. I. Dodson, S. Ryan, R. Tollrian, and W. Lampert, Individual swimming behavior of daphnia: Effects of food, light and container size in four clones, J. Plankton Res. **19**, 1537 (1997).

[82] T. C. O'Keefe, M. C. Brewer, and S. I. Dodson, Swimming behavior of daphnia: Its role in determining predation risk, J. Plankton Res. **20**, 973 (1998).

[83] M. M. Wilhelmus and J. O. Dabiri, Observations of large-scale fluid transport by laser-guided plankton aggregations, Phys. Fluids **26**, 101302 (2014).

[84] T. Gorgues, O. Aumont, and L. Memery, Simulated changes in the particulate carbon export efficiency due to diel vertical migration of zooplankton in the north atlantic, Geophys. Res. Lett. **46**, 5387 (2019).

[85] M. Tanaka, A. Genin, Y. Endo, G. N. Ivey, and H. Yamazaki, The potential role of turbulence in modulating the migration of demersal zooplankton, Limnol. Oceanogr. **66**, 855 (2021).

[86] P. J. Franks, B. G. Inman, J. A. MacKinnon, M. H. Alford, and A. F. Waterhouse, Oceanic turbulence from a planktonic perspective, Limnol. Oceanogr. **67**, 348 (2022).

[87] W. M. Durham, J. O. Kessler, and R. Stocker, Disruption of vertical motility by shear triggers formation of thin phytoplankton layers, Science **323**, 1067 (2009).

[88] N. Mousavi, J. Qiu, B. Mehlig, L. Zhao, and K. Gustavsson, Efficient survival strategy for zooplankton in turbulence, Phys. Rev. Res. **6**, L022034 (2024).

[89] J. Morales, P. Muñoz, D. Noto, H. N. Ulloa, and F. Guzmán-Lastra, Agent-based modeling of swarm dynamics of motile photokinetic organisms, Zenodo (2026), doi: 10.5281/zenodo.19152025.